Modeling Human Difference Threshold in Perceiving Mechanical Properties from Force

Fu, Wei; Landman, Annemarie; van Paassen, Rene; Mulder, Max

DOI
10.1109/THMS.2018.2844212

Publication date
2018

Document Version
Accepted author manuscript

Published in
IEEE Transactions on Human-Machine Systems

Modeling Human Difference Threshold in Perceiving Mechanical Properties from Force

Wei Fu, Annemarie Landman, M. M. (René) van Paassen, *Senior Member, IEEE*, and Max Mulder, *Member, IEEE*

***Abstract*—We discuss an extension of the basic principles underlying the human haptic just noticeable difference (JND) in perceiving a manipulator's mechanical properties from force feedback. Two cases are studied: 1) the JND in perceiving the stiffness of manipulators with various masses; 2) the JND in perceiving the damping of a combined mass-spring-damper system with varying stiffness and mass. The extended JND laws are obtained through mapping psychophysical findings to JND formulations based on frequency response functions. We first present two human-factor experiments in which subjects discriminated between different levels of manipulator stiffness/damping while moving the manipulator with a prescribed sinusoidal deflection. For the two testing cases both JNDs violate Weber's law: Due to the increases in mass, the normalized stiffness JND (the Weber fraction) decreases as the reference stiffness level increases; The damping JND for a constant reference damping increases with higher combined responses of stiffness and mass. On the basis of weighting the frequency response magnitude of mechanical properties, we performed model identification that fit the experimental observations, and extended the JND laws for the two testing cases. Our extended JND laws indicate that: 1) stiffness and mass affect the stiffness JND in the same way, the stiffness JND is a fixed proportion of the combined frequency response of stiffness and mass; 2) the frequency response magnitude of the damping JND is a fixed proportion of the frequency response magnitude of the combined system (the mass-spring-damper system).**

***Index Terms*—Mechanical properties, Just Noticeable Difference, Frequency response function, Haptic perception threshold**

I. Introduction

In many manual control tasks, a control manipulator serves as the haptic interface between humans and machines. In bilateral tele-operation, the human operator uses the manipulator to command the motion of the slave robot in the remote environment, while estimating the mechanical properties of the environment – stiffness, mass and damping – through the force feedback. In flight, the pilot controls the attitude of the aircraft by steering, and changes in the aerodynamic force acting on the control surface, when fed back to the pilot, result in changes in the mechanical properties of the manipulator.

Rendering the proper dynamic information of tasks through the force feedback is of primary importance to a haptic interface. However, the desired information of stiffness, mass and damping conveyed by the force feedback is inevitably distorted. Probable causes are limitations from the digital control systems and actuators, and transmission time delays that occur in many tele-operation systems. Similar to perception limitations in other human modalities, a change in a haptic stimulus must also exceed a certain level to become perceivable. This level, the minimal perceivable change, is referred to as the Just Noticeable Difference (JND).

Knowledge on how large a difference in the force feedback must be to result in different human perception of mechanical properties, i.e., the JND in perceiving manipulator stiffness, damping and mass, is important to the design of haptic interfaces. This can be used to balance the trade-off between transparency and stability of bilateral tele-operation systems [1]–[4], to assess the fidelity of control loading devices of flight training simulators [5], [6], and is also relevant for the design of haptic support systems in vehicle control [7]–[9].

In the last few decades, many investigations have been carried out on this topic. The majority of work is based on the assumption that each mechanical property – stiffness, mass or damping – is rendered in isolation. Under this assumption, the human JND can be expressed with Weber's law [10]–[14], which states that the JND is a fixed proportion of the reference stimulus level. However, the manipulator dynamics in manual control tasks are usually defined by more than one mechanical property. In that case, Weber's law does not apply to the corresponding JNDs, largely limiting the applicability of the present research. For example, the JND in perceiving the manipulator damping increases for manipulators with a higher mass or stiffness [15]. It seems that the perceptions of different properties are *coupled*, and that a change in one property can be "masked" by variations in the other two properties.

To take better advantage of this perceptual characteristic for the design of haptic interfaces, an extension of the JND law is necessary for cases when multiple mechanical properties define the manipulator dynamics. In this paper, we address the following two research questions:

1) When stiffness and mass are rendered simultaneously, how do changes in the manipulator mass affect human JND in perceiving manipulator stiffness from the force feedback?
2) When a combined mass-spring-damper system is rendered, how do the manipulator mass and stiffness affect human JND in perceiving the manipulator damping?

In Section II we will argue why these two cases, among many other potential variations, are the most important to address. In this paper we will build mathematical models to extend the JND laws for these two cases. We apply psychophysical findings to formulate the JND using the control-theoretic frequency response function (FRF). In addition, we

The authors are with the faculty of Aerospace Engineering, Delft University of Technology, 2629 HS Delft, The Netherlands. E-mail: {W.Fu-1; H.M.Landman; M.M.vanPaassen; M.Mulder}@tudelft.nl

will decompose the characterization of the JND into investigations with individual manipulator excitation frequencies, and select a representative frequency, 6 rad/s, for the investigation in this study.

The contributions of this paper are twofold:

1) An extension of the stiffness JND law: (16).
   - From a human-factor experiment, we find that the JND in manipulator stiffness violates Weber's law when the manipulator mass varies. The Weber fraction for stiffness decreases with increasing manipulator mass.
   - We successfully model the stiffness JND by weighting the frequency responses of stiffness and mass. In the frequency domain, the stiffness JND is a fixed proportion of the combined response of the stiffness and mass.
2) An extension of the damping JND law: (17).
   - We find that the JND in perceiving manipulator damping violates Weber's law when the joint response of manipulator mass and stiffness varies. The Weber fraction for damping increases when the joint response of the stiffness and mass is higher.
   - The damping JND law is extended using the most accurate model from three candidate models. In the frequency domain, the response of the damping JND is a fixed proportion of the response of the combined mass-spring-damper system.

The remainder of this paper is organized as follows: In the next section, we elaborate the two research questions of this study. In Section III, we design conditions for the human factor experiment, and propose candidate models for the corresponding JNDs. The experimental setup is given in Section IV. The experiment results are given in Section V. We extend the JND laws for the two considered cases and validate the extension in Section VI. Our work is further discussed in Section VII and concluded in Section VIII.

II. Research Questions and Objectives

In many cases, the dynamics of a control manipulator can be adequately described as a mass-spring-damper system. Changing a manipulator deflection angle resembles moving a mass that is connected with a spring and a damper to an infinitely stiff basis. The inertial mass (m), the damping coefficient (b) and the spring coefficient (k), determine the system's harmonic torque response to a given deflection through a frequency response function (FRF):

$$\begin{aligned} H(\omega) &= \frac{T(\omega)}{\Theta(\omega)} = G_k(\omega) + G_m(\omega) + G_b(\omega) \\ &= \underbrace{k - m\cdot\omega^2}_{\Re H(\omega)=G_k(\omega)+G_m(\omega)} + \underbrace{jb\cdot\omega}_{\Im H(\omega)=G_b(\omega)} \end{aligned} \tag{1}$$

Here $T(\omega)$ and $\Theta(\omega)$ denote the Fourier transforms of the torque $\tau(t)$ and deflection angle $\theta(t)$, respectively. It follows that $T(\omega)$ is a combination of three torque components, which are determined by the frequency responses of stiffness, mass and damping: G_k, G_m and G_b. Without loss of generality, in this section we refer to torque as force for the sake of clarity.

The majority of past research investigated the JND when each property is rendered in isolation. In such cases only one term (G_k, G_m or G_b) is active in (1). A manipulator defined by such dynamics has a fixed phase difference between its movement and force response. For example, as illustrated in the upper plot of Fig. 1, a manipulator behaving like a spring or mass, when moved as a sinusoidal deflection, it yields a force *synchronous* to its deflection angle. The forces generated by these two properties have opposite directions, however. The force generated by a damper-like manipulator is proportional to the manipulator *velocity*, with the ratio b (the damping level). So in response to a sinusoidal input it has a 90-degrees phase difference to the deflection angle. A change in these isolated mechanical properties only changes the force amplitude but never changes the phase characteristic. Hence, a human operator can identify the property's type from the phase characteristics, and changes in the amplitude (strength) of the force give him/her accurate indication of changes in this property. In these cases, the JND in perceiving a mechanical property can be described with Weber's law:

$$\frac{\Delta I_{jnd}}{I} = c, \tag{2}$$

where I and ΔI_{jnd} respectively denote the reference property (stimulus) and the JND; c denotes a constant.

However, in more general and relevant cases where a manipulator behaves as a *combined* system, the force response is affected by multiple mechanical properties *simultaneously*. The lower plot of Fig. 1 illustrates the force of a combined mass-spring-damper system: the sum of the forces resulting from stiffness, mass and damping. The magnitude or the phase characteristics of this combined force no longer reflects the characteristics of individual properties that were discussed above. And a change in any of the three mechanical properties changes both the magnitude and phase of this combined force. In these cases, identifying a change in one mechanical property

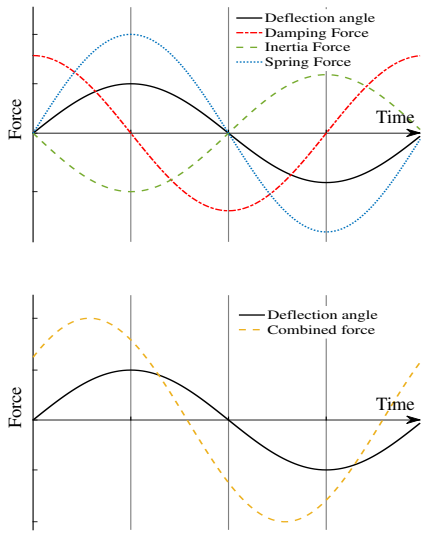

Fig. 1. An illustration of the stationary force responses of different mechanical properties, excited by a sinusoidal deflection angle. (upper): Isolated force responses of the three mechanical properties. (lower): The force response of a combined mass-spring-damper system.

requires a discrimination of the force caused by this property from the forces caused by the other ones. The accuracy of this identification depends on the accuracy of extracting information of individual properties from the perception of the combined force.

As can be seen in (1), we distinguish the real and imaginary components in a manipulator's FRF, $\Re H$ and $\Im H$. Our two research questions directly follow from this equation:

1) The responses of stiffness and mass are linearly coupled, constituting a joint response: the real part $\Re H$. This causes us to wonder whether humans can still isolate the response (the force) of either property from the joint response. In order to investigate this possible coupling, the JND in perceiving stiffness of manipulators with various mass will be studied, for the zero damping case.
2) Damping determines the imaginary part $\Im H$, and it responds asynchronously to the joint response of stiffness and mass $\Re H$. Humans should be able to extract the damping force from the combined total force, but the accuracy may be affected. To quantify the possible joint effect of stiffness and mass on the accuracy of perceiving the damping, the JND in perceiving damping of combined mass-spring-damper systems with various $\Re H$ settings will be studied.

In order to extend the JND laws for these two cases, we will perform system identification to estimate the weights of frequency-response contributions of the three mechanical properties. As can be seen from (1), the frequency of excitation ω also plays an important role. This suggests that the characterization of the corresponding JNDs could be performed by investigation at individual frequencies using individual sinusoidal manipulator movements. We start our investigation at a single frequency of excitation, representative of frequencies utilized by participants when a manipulator motion profile can be freely chosen, in this case 6 rad/s (about 1 Hz). Details of the used manipulator movement is given in Section IV-C.

III. Candidate models and experiment design

In this section, we design the conditions for two human-factor experiments where the two research questions are addressed. Here we define Δk_{jnd} and Δb_{jnd} as the JNDs in stiffness and damping, their FRFs are:

$$\begin{aligned} \Delta G_{k,jnd}(\omega) &= \Delta k_{jnd} \\ \Delta G_{b,jnd}(\omega) &= \Delta b_{jnd} \cdot (j\omega) \end{aligned} \tag{3}$$

In the next two subsections we propose candidate models of $\Delta G_{k,jnd}$ and $\Delta G_{b,jnd}$, for the system identification purpose.

A. Case 1: stiffness JND

1) Experimental Conditions: In order to study the effect of mass on the stiffness JND, we will measure the stiffness JND for three conditions which vary in manipulator stiffness and mass. The manipulator damping was kept at zero in all testing conditions to solely focus on the effect of mass. Throughout this paper, we label the three conditions as $C_k i$ $(i = 1, 2, 3)$, of which the settings are given in Table I. The stiffness and mass settings chosen are within the typical manipulator setting range for manual control tasks [16]. Note that all mechanical properties are defined with the rotational convention, since the manipulator used in the experiments generates torque to its deflection (see details of the device in Section IV-A).

TABLE I
Conditions of the two experiments

		Stiffness k (Nm/rad)	Mass m (kgm^2)	Damping b $(Nm \cdot s/rad)$	Ratio r_i $\frac{\lvert\Re H\rvert}{\lvert G_b\rvert}$
Stiffness JND	C_k1	2.50	0.0100	0	-
	C_k2	3.75	0.0447	0	-
	C_k3	5.00	0.0794	0	-
Damping JND	C_b1	0.36	0.01	0.25	0.00
	C_b2	1.11	0.01	0.25	0.50
	C_b3	1.86	0.01	0.25	1.00
	C_b4	2.61	0.01	0.25	1.50
	C_b5	3.36	0.01	0.25	2.00

2) Model: In case humans can accurately extract the force caused by the stiffness property, the stiffness JND will follow Weber's law, i.e., $\Delta G_{k,jnd}$ is a fixed proportion of G_k. In case mass affects the perception of stiffness, $\Delta G_{k,jnd}$ will be determined by both G_k and G_m.

The following model of $\Delta G_{k,jnd}$ will be used to estimate the effect of mass:

$$\Delta \hat{G}_{k,jnd} = p_{s,1} \cdot G_k + p_{s,2} \cdot G_m \tag{4}$$

Here, $p_{s,1}$ and $p_{s,2}$ denote the weights of the two factors. The Weber fraction for stiffness can be expressed as follows:

$$\hat{W}_k = \frac{\Delta \hat{k}_{jnd}}{k} = \frac{|\Delta \hat{G}_{k,jnd}|}{|G_k|} = \frac{p_{s,1} \cdot k - p_{s,2} \cdot m\omega^2}{k} \tag{5}$$

Estimates of the two weights can be obtained from the measurements of the stiffness JND. The value of $p_{s,2}$ will indicate the exact relation between the stiffness JND and mass.

B. Case 2: damping JND

1) Experimental Conditions: As already discussed above, the damping property responses are asynchronous to the stiffness and mass properties. In the complex plane its frequency response is perpendicular to the other two mechanical properties, so formulating the damping JND may require a more complex model than the linear model used for the stiffness JND. We will therefore propose three candidate models in the next subsection. To obtain sufficient measurements for an accurate parameter estimation and a fair model comparison, we measure the damping JND at five testing conditions. These conditions have the same reference damping level but five different levels of $\Re H$. Since the damping JND follows Weber's law in case the damping is rendered in isolation, one level of damping is sufficient to show whether this law is violated or not when varying the other two properties. The chosen damping level is commonly used in manual control research setups [16]. We label the conditions as $C_b i$ $(i = 1, \ldots, 5)$ throughout this paper, they define different ratios (r_i) between $|\Re H|$ and $|G_b|$ $(|\Im H|)$ at the desired excitation frequency (6 rad/s), as shown in Table I.

A change in $\Re H$ may account for changes in either or both stiffness and mass, so the five conditions will allow us to determine the joint effect of stiffness and mass on the damping JND. When considered at a single frequency, a change in $\Re H$ can be obtained by only adjusting the stiffness, we thus used different manipulator stiffness settings to obtain the desired variations in $\Re H$.

2) Candidate Models: The Weber fraction for damping (W_b) can be derived from the frequency response of the damping JND ($\Delta G_{b,jnd}$):

$$W_b = \frac{\Delta b_{jnd}}{b} = \frac{|\Delta G_{b,jnd}|}{|G_b|} \tag{6}$$

The first condition marks a zero effect of $\Re H$, and is used as the baseline. In case no effects of $\Re H$ exist, W_b will remain invariant over the five conditions. In case $\Re H$ affects the damping JND, differences in measurements will be found between the baseline and other conditions. By observing how W_b changes with r, the exact effect can be studied. To quantify the possible effects, we propose three candidate models.

An intuitive way would be to estimate the weights of the two factors separately. Thus we define N_1 and N_2 as the weighted effects of G_b (determined by damping) and $\Re H$ (determined by stiffness and mass), respectively:

$$N_1 = p_{b,1} \cdot |G_b| \quad , \quad N_2 = p_{b,2} \cdot |\Re H| \tag{7}$$

Here, $p_{b,1}$ and $p_{b,2}$ denote the weights of the two factors.

The First Model: We assume a simple relation, namely that the two factors determine ΔG_b through a linear addition:

$$|\Delta \hat{G}_{b,jnd}| = N_1 + N_2 = |G_b| \cdot (p_{b,1} + p_{b,2} \cdot r) \quad , \tag{8}$$

with r the ratio of $|\Re H|/|G_b|$. Substituting the above equation into (6), we get the estimated Weber fraction for damping:

$$\hat{W}_b = \frac{|\Delta \hat{G}_{b,jnd}|}{|G_b|} = p_{b,1} + p_{b,2} \cdot r \tag{9}$$

The Second Model: As can be seen from (1), the two factors, G_b (imaginary part) and $\Re H$ (real part), are perpendicular to each other in the complex plane. Considering this characteristic, one could assume that these factors affect the JND threshold through a weighted power addition:

$$|\Delta \hat{G}_{b,jnd}| = \sqrt{N_1^2 + N_2^2} = |G_b| \cdot \sqrt{p_{b,1}^2 + p_{b,2}^2 \cdot r^2} \tag{10}$$

Here N_1 and N_2 are defined by (7)). Substituting the above equation into (6)), results in:

$$\hat{W}_b = \frac{|\Delta \hat{G}_{b,jnd}|}{|G_b|} = \sqrt{p_{b,1}^2 + p_{b,2}^2 \cdot r^2} \tag{11}$$

The Third Model: In practice, the estimation of the damping JND using two different factors can be tedious. It will be more efficient if the damping JND can be described with a single factor, in a way similar to Weber's law. We therefore formulate the damping JND using the FRF of the combined system ($H(\omega)$) to include the effects of both G_b and $\Re H$:

$$\begin{aligned} |\Delta \hat{G}_{b,jnd}| &= p_b \cdot |H| \\ &= p_b \cdot |G_b| \cdot \sqrt{r^2 + 1} \end{aligned} \tag{12}$$

Fig. 2. The apparatus used in the JND experiment. The side-stick manipulator and the LCD screen are marked by white rectangles. The manipulator could be deflected laterally (left/right) like a joystick. The LCD screen only displays the visual presentation of the tracking task.

This model estimates the frequency response of the damping JND as a fixed proportion of the combined system's frequency response. Substituting the equation above into (6), we get:

$$\hat{W}_b = \frac{|\Delta \hat{G}_{b,jnd}|}{|G_b|} = p_b \cdot \sqrt{r^2 + 1} \tag{13}$$

IV. Experimental setup and method

A. Apparatus and participants

The experiments were performed in the Human-Machine Interaction Laboratory at the faculty of Aerospace Engineering, TU Delft. An illustration of the devices is given in Fig. 2. An admittance-type side-stick manipulator driven by an electro-hydraulic motor was used in the experiment. The manipulator could move in the left/right direction (lateral) like a joystick. Position of the manipulator and moment on the manipulator are led through presample filters (bandwidth = 200 HZ) before being digitized at 2500 HZ and read into the laboratory computer. The manipulator's control system is executed at 2500 HZ, and effective position following bandwidth is around 40 HZ, so the torque-to-deflection manipulator dynamics specified by (1) can be accurately rendered to the human operator at the desired frequency of excitation (6 rad/s, approximately 1 HZ).

The manipulator is supplied with a handle, diameter 35 mm, with grooves for placement of the fingers. When a hand is correctly placed on the handle, the center of the hand lies 90 mm above the manipulator rotation axis. The settings of the mass, spring and damper coefficients (m, k and b) of the rendered manipulator dynamics could be configured according to different conditions. An LCD screen, placed in front of the subject, was used to help subjects follow the prescribed sinusoidal manipulator movement (detailed description of the visual presentation is given in Section IV-C). Subjects were asked to wear an active noise suppression headphone (David Clark H10-66XL), to cancel possible auditory cues.

Eight human subjects participated in both experiments. All participants were right-handed and reported no hand/arm impairment history. An informed consent form was signed before experiments. This study was approved by the Human Research Ethics Committee of Delft University of Technology.

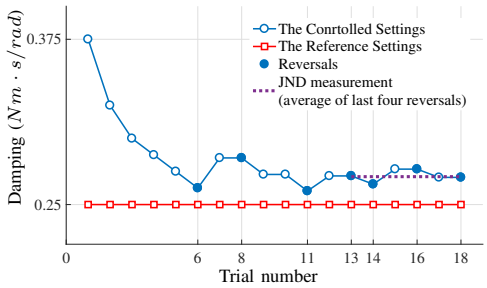

Fig. 3. An example of the staircase procedure obtained in the damping JND experiment. One up/one down procedure was used before the first reversal for a quick convergence. The reference damping setting is fixed in the whole procedure, and the controlled damping setting is adjusted by subjects' responses.

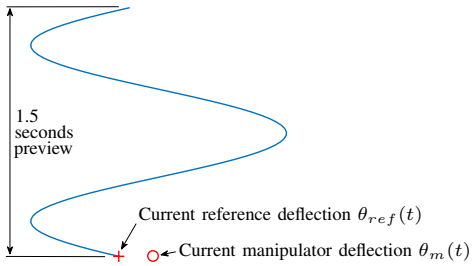

Fig. 4. The visual presentation of the preview tracking task shown on the LCD screen. To reduce the tracking error (the difference between "+" and "○") exampled here, the subject has to push the manipulator towards the left.

B. Procedure

In this study, only the upper JNDs were investigated. The JNDs were measured by a one-up/two-down adaptive staircase procedure [17]. The ratio of the down stepsize to the up stepsize was 0.5488. The measured JND was in accordance with 80.35% correct performance [18]. An example of the staircase procedure is shown in Fig. 3.

For each condition, a complete staircase procedure was performed by the subject. It generally consisted of approximately 20 trials. Each trial consisted of two 6.3-second simulations. In one of the two simulations in each trial, the side-stick manipulator was configured with a reference setting, and in the other simulation it was configured with a controlled setting. The reference manipulator setting for all trials in a staircase procedure was fixed and defined by one of the conditions in Table I. The controlled manipulator setting only differed from the reference setting in the tested mechanical property S (stiffness or damping) by an adjusted increment δS.

In each simulation, the subject was asked to move the manipulator with the prescribed sinusoidal deflection while perceiving the manipulator dynamics (the prescribed manipulator deflection will be elaborated in Section IV-C). After each trial, the subject was asked to report in which of the two simulations he or she experienced a higher level of manipulator stiffness (in the stiffness JND experiment) or manipulator damping (in the damping JND experiment). The sequence in which the two simulations of each trial were presented to the subject was random, based on a prior probability of 0.5. The δS for the next trial was increased when a subject gave a wrong answer (e.g., the 6th, 11th, 14th and 18th trial in Fig. 3), and was reduced when the subject gave correct answers in two consecutive trials. Here we define a reversal as the trial where the staircase curve changes direction (see solid markers in Fig. 3). The procedure ended when the 7th reversal occurred, or when the total number of trials reached 40. The JND was defined as the average of the last four reversals (trial 13, 14, 16 and 18 in the figure), as illustrated by the purple dashed line in Fig. 3.

Each subject performed the two experiments on two separate days in a random order. Sufficient training preceding the experiment was performed to improve the tracking performance (described in Section IV-C) and to familiarize subjects with the comparison task.

C. Prescribed manipulator movement

In order to ensure that the discrimination task would be conducted with the prescribed single-frequency sinusoidal manipulator movement, subjects performed a preview tracking task. The visual presentation of the tracking task is illustrated in Fig. 4. Note that only the blue curve and the two red symbols ("+" and "○") in this figure were actually shown to the subject. This display was provided on an LCD screen placed in front of the subject (marked by white rectangle in Fig. 2). The reference manipulator deflection $\theta_{ref}(t)$ (shown as "+" on the display) was calculated using:

$$\theta_{ref}(t) = \begin{cases} \alpha \cdot \theta_0(t)\,, \text{ if } t < 1.0 \\ \beta \cdot \theta_0(t)\,, \text{ if } t > 5.3 \\ \theta_0(t)\,, \text{ else} \end{cases} \tag{14}$$

where, $\theta_0(t) = 0.37 \cdot \sin(6t)\,,\ \alpha = t\,,\ \beta = 6.3 - t.$

The first and last seconds were used as fade-in/out phases, during which the amplitude of the reference movement gradually in/decreases. The current manipulator deflection $\theta_m(t)$ applied by the subject was measured and shown as "○" on the display. To perform the tracking task, the subject was instructed to minimize the error between "○" (the current manipulator deflection $\theta_m(t)$) and "+" (the current reference deflection $\theta_{ref}(t)$). These two symbols can only move horizontally. The visual preview, shown as a winding curve (blue line), contains 1.5-second future information of the reference deflection θ_{ref}. It moves downwards as time progresses.

D. Model Parameter Estimation and Validation

Parameters of the models proposed in Section III can be estimated using the JND measurements. The estimation involves the minimization of a weighted, output-error based criterion J:

$$J = \sum_{i=1}^{N} f(\varepsilon_i^2, \sigma_{\overline{x},i}) \qquad \text{where} \quad \varepsilon_i = \lambda_i - \tilde{W}_i(\hat{p}, \tilde{\omega}_i). \tag{15}$$

Here, N denotes the total number of conditions (N=3 for the stiffness JND experiment and N=5 for the damping JND

TABLE II
STIFFNESS JND MEASUREMENTS AND POST-HOC RESULTS

Conditions m | k	Normalized JND: $\frac{\Delta k_{jnd}}{k}$ (%)	Normalized JND: Post-Hoc Sig. (p value)	Absolute JND: Δk_{jnd} (Nm/rad)
C_k1: 0.0100 | 2.50	10.9 ± 2.1	C_k1 vs. C_k2: .033*	$0.27 \pm .068$
C_k2: 0.0447 | 3.75	6.9 ± 0.9	C_k2 vs. C_k3: .018*	$0.26 \pm .029$
C_k3: 0.0794 | 5.00	5.2 ± 1.6	C_k3 vs. C_k1: .009*	$0.26 \pm .059$

Units of variables m and k are given in Table I. Symbol * indicates that the result of the post-hoc T-test is significant (after a Holm-Bonferroni correction).

TABLE III
DAMPING JND MEASUREMENTS AND CONTEST TEST RESULTS

Conditions damping b | ratio r	Normalized JND: $\frac{\Delta b_{jnd}}{b}$ (%)	Contrast test Baseline C_b1 Sig. (p value)
C_b1: 0.25 | 0.0	9.8 ± 2.0	-
C_b2: 0.25 | 0.5	10.6 ± 2.3	.573
C_b3: 0.25 | 1.0	12.6 ± 4.4	.304
C_b4: 0.25 | 1.5	16.3 ± 2.9	.011*
C_b5: 0.25 | 2.0	20.8 ± 3.9	.000*

The unit of damping b is given in Table I. The first condition C_b1 was used as the baseline condition in the contrast test. Symbol * indicates that the result of the contrast test remains significant after Holm-Bonferroni correction.

TABLE IV
ACTUAL FREQUENCY OF EXCITATION AND THE RESULTANT RATIO r

	Exp 1			Exp 2				
	C_k1	C_k2	C_k3	C_b1	C_b2	C_b3	C_b4	C_b5
$\tilde{\omega}$	5.98	6.00	6.02	5.96	5.97	5.98	5.97	5.98
$\tilde{r}$	-	-	-	.003	.505	1.00	1.51	2.00

experiment). The subscript i of all variables denotes the condition number. $\hat{p}$ is the parameter set that needs to be estimated. λ denotes the sample mean of the measured Weber fraction. $\sigma_{\overline{x}}$ denotes the corresponding standard error (the standard deviation of the sample mean) corrected for between-subjects variability. $\hat{W}$ is the estimate of the Weber fraction given by the candidate models. $\tilde{\omega}$ denotes the actual manipulator movement frequency that subjects generated during the experiment. A 'leave-one-out' cross validation procedure is employed to select the best candidate model for the damping JND.

V. RESULTS AND ANALYSIS

Subjects performed the tracking task with considerable accuracy. The manipulator was excited at the desired frequency, as can be seen from the actual frequency of excitation $\tilde{\omega}$ determined from the measured data as listed in Table IV. Thereby the JND measurements accurately reflect the effects of the testing factors at the desired testing condition. In the following two sub-sections, we discuss the results of the two experiments.

A. Experiment 1: stiffness JND

The JND measurements are shown as Weber fractions (the normalized JND: $\Delta k_{jnd}/k$) with the sample mean and $\pm 95\%$ confidence intervals corrected for between subjects variability, in Table II. The result of a one-way repeated measures ANOVA shows that the effect of different condition settings on this fraction is significant ($F(2,14) = 10.9, p < 0.05$). Post-hoc pairwise comparisons (after Holm-Bonferroni correction) reveal that each condition is significantly different from the other two, see Table II. However, the *absolute* values of the stiffness JND: Δk_{jnd}, of the three conditions are approximately the same (see Table II), and seem unaffected by the different settings (one-way repeated measures ANOVA: $F(2,14) = 0.54, p = 0.95$).

This result shows that our subjects were able to detect a *fixed absolute amount* but *smaller proportion* of stiffness change from the force when the reference stiffness level increases. This violates Weber's law given in (2). Such a violation is caused by the variation in the mass: apparently a higher mass level leads to a lower *normalized* stiffness JND.

B. Experiment 2: damping JND

Table III shows the measurements of the damping JND with sample means and $\pm 95\%$ confidence intervals corrected for between-subject variability. The damping JND shows a clear increasing trend for higher $\Re H$. This means that the least detectable damping change becomes *a larger proportion* of the reference damping when the joint response of stiffness and mass increases. This violates Weber's law.

A one-way repeated-measures ANOVA shows that the effect of r on the damping JND is significant: $F(4,28) = 7.75, p < 0.05$. Contrast tests (with Holm-Bonferroni correction), comparing conditions $C_b2{:}5$ to the baseline condition C_b1, reveal the effect of r to be significant when r is larger than 1.5, see Table III. These results confirm that the *joint* response of stiffness and mass affects the damping JND, although this effect is signiifcant only for higher values of r.

VI. EXTENSION OF THE JND LAWS

In this section, we extend the JND laws for the two testing cases: 1) human JND in perceiving the stiffness of linear systems with various mass settings and zero damping; 2) human JND in perceiving the damping of combined systems with various joint responses of stiffness and mass. We first estimate the model parameters using the experimental data listed in Tables II - IV with the procedure explained in Section IV-D, then extend the corresponding JND laws for the two cases accordingly. We also investigate our subjects' strategies used for the discrimination task, to explain the underlying principle of the experimental observations, and also to backup the proposed extensions of the JND law.

A. Extension of stiffness JND law

1) Model Identification: The estimated parameters of the model (5) are given in Table V. With these two parameters,

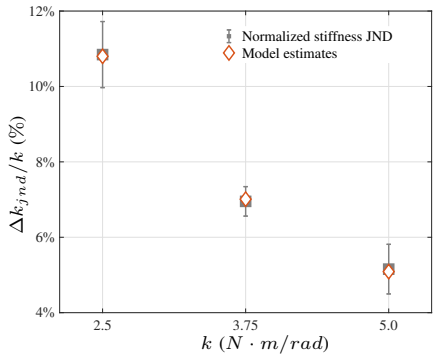

Fig. 5. Normalized stiffness JND measurements and model estimates. The measurements are shown with sample means (gray square) and standard errors corrected for between subject variability (error bars).

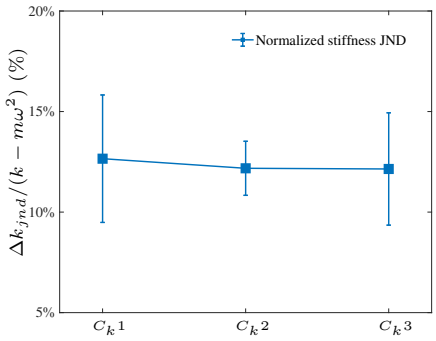

Fig. 6. The stiffness JND Δk_{jnd} normalized to the combined frequency response of stiffness and mass. Error bars represent the 95% confidence interval corrected for between subject variability.

the model provides accurate estimates of the observed stiffness JNDs, as shown by the red diamonds in Fig. 5. The weights of G_k and G_m (0.126 and 0.130) are practically identical, indicating that the stiffness and mass affect the stiffness JND in the same manner in the frequency domain. Hence, our model can be simplified to become:

$$\frac{\Delta G_{k,jnd}}{G_{k+m}} = \frac{\Delta k_{jnd}}{(k - m\omega^2)} = p_s\,, \tag{16}$$

with a single ratio constant p_s being 0.124. Here we use G_{k+m} to represent the combined frequency response of stiffness and mass: $G_k + G_m$. As can been seen, this simplified model replaces the reference property in the denominator of (2) with this combined response.

The stiffness JND can still be described with Weber's law in the frequency domain, if the reference stimulus is defined from a different perceptive. If we define the reference stimulus as the *combined* frequency response of stiffness and mass, the stiffness JND becomes a fixed proportion of this stimulus.

This can be validated by the experimental data, and in Fig. 6 we plot the stiffness JND that is normalized to the newly defined stimulus: G_{k+m}. When the JND is expressed in this way, no statistical differences can be observed (one-way repeated measures ANOVA: $F(2, 14) = 0.04, p = 0.96$).

Equation (16) enables us to extend the JND law for the first testing case: the JND in perceiving the stiffness of systems with various mass and zero damping. In addition, this extension does not conflict with the original law given in (2). When the excitation frequency ω approaches zero, or the manipulator mass m is negligible, the two laws become identical.

TABLE V
MODEL PARAMETER ESTIMATES

Stiffness JND		Damping JND				
		Model 1		Model 2		Model 3
$p_{s,1}$	$p_{s,2}$	$p_{b,1}$	$p_{b,2}$	$p_{b,1}$	$p_{b,2}$	p_b
.126	.130	.086	.053	.095	.090	.092

2) Principle Investigation: From the experiment we found that a variation in manipulator mass affects the least detectable *proportion* of difference in stiffness, however, not the *absolute value*. With a closer examination of the condition settings in Table I, it can be found that the newly defined reference stimulus: G_{k+m} in (16), is identical for all three conditions at the prescribed excitation frequency (6 rad/s). Since the extended JND law indicates that the stiffness JND is a fixed proportion of G_{k+m}, the invariant *absolute value* is therefore a consequence of our experiment settings.

The principle governing how our subjects estimated a stiffness change can help us to explain the extended law of the stiffness JND. After the experiment, we asked our subjects to reflect on their strategies for the discrimination task. All of them indicated that, to identify the stiffness difference between the two simulations of each trial, they compared the forces they perceived at the *extremes* of the manipulator deflection (max($|\theta_{ref}|$): when $\theta_{ref}(t) = \pm 0.37\ rad$). As discussed in Section II, it is at this deflection where both the spring and inertia forces become maximal. So the force that subjects used to estimate the stiffness is actually the maximum of a *combined* force, caused by stiffness and mass properties. Apparently, our subjects *could not separate* the spring force and the inertia force when these two force components are combined, such that the perceived change is a change in the *combined* response of these mechanical properties.

This manifests that our subjects only perceive the "effective stiffness" [19] rather than the true stiffness. Here, the "effective stiffness" equals the amount of the positive real projection of the system's FRF, and in our case it is the newly defined stimulus: G_{k+m}. To better illustrate this, we plot G_{k+m} at the prescribed frequency in the complex plane, and this case as a complex vector shown as the red line in Fig. 7.

This vector describes how the system responds to a sinusoidal excitation signal [20]. Its magnitude and phase angle define, respectively, the amplitude difference and the phase difference between the movement and force. With our experimental settings, the three conditions have identical vectors, all located on the positive real axis. This horizontal vector generates an "effective spring force" proportional to the deflection angle of the manipulator. Thus, our subjects' strategy is equivalent to comparing the positive real projection of the system: the effective stiffness. Since the force difference threshold follows Weber's law, perceiving the change in the

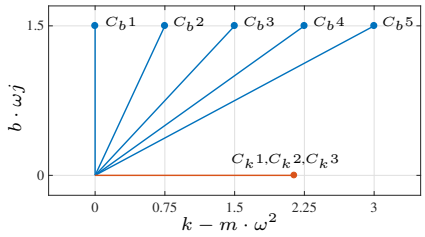

Fig. 7. Frequency responses at 6 rad/s, of different condition settings of the two experiments, plotted in the complex plane.

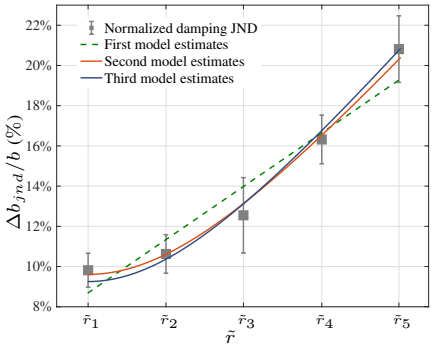

Fig. 8. The normalized damping JND measurements, and estimates from the three candidate models. The measurements are shown with sample means (gray square) and standard errors (error bars) corrected for between subject variability.

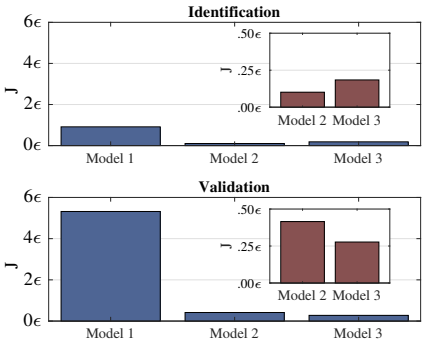

Fig. 9. Scaled fitting errors (outputs of cost functions in (15)) of the three candidate models, given by the identification and validation processes of the "leave-one-out" method. ϵ denotes the scaling factor. The small plots are zoom-in comparisons between the second and third model.

maximum of the "effective spring force" leads the stiffness JND to be a fixed proportion of the effective stiffness G_{k+m}.

B. Extension of damping JND law

1) Model Identification and Selection: The estimated parameters of the three candidate models are shown in Table V. Model predictions using these parameter estimates are shown in Fig. 8 together with the JND measurements. The first model, based on a linear structure, does not accurately fit the measurements. Its estimation error is acceptable, but the validation error is high (see Fig. 9). The second and third models, based on nonlinear structures, both provided good

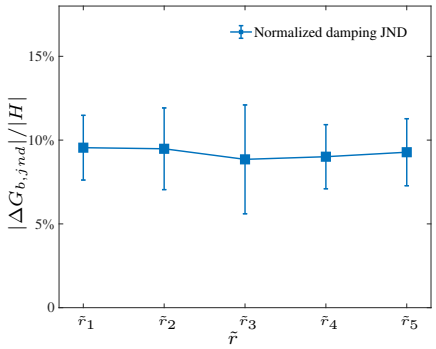

Fig. 10. The damping JND frequency response magnitude normalized to the combined system magnitude. Error bars represent the 95% confidence interval corrected for between subject variability.

predictions with similar low errors for both identification and validation. In addition, the values of the two parameters of the second model are almost identical. In this case, (11) resembles (13), equalizing the second and third models.

The third model formulates the damping JND as a fixed proportion of the combined system in the frequency domain. This can be further evaluated by normalizing the measured $|\Delta G_{b,jnd}|$ to the frequency response of the combined system $|H|$, as shown by Fig. 10. No significant difference can be found among the five conditions (one-way repeated measures ANOVA: $F(4, 28) = 0.07, p = 0.99$).

With the third model, the damping JND can be expressed with Weber's law in the frequency domain if we consider the reference stimulus as the combined system, that is, the least amount of a damping change that makes the system feel differently, is a fixed proportion of the system's magnitude:

$$\frac{|\Delta G_{b,jnd}|}{|H|} = \frac{|\Delta b_{jnd} \cdot \omega j|}{|m \cdot (\omega j)^2 + b \cdot \omega j + k|} = p_b \qquad (17)$$

The above formula enables us to extend the JND law for the second testing case: the JND in perceiving the damping of combined systems with various stiffness and mass. This extension does not conflict with the original JND law given in (2). When both manipulator stiffness and mass are negligible, this extended law is identical to the original one.

2) Principle investigation: From the experiment we found that the damping JND becomes higher when a higher joint response of stiffness and mass is rendered. Similar to the first experiment we asked our subjects about their discrimination strategy. Subjects reported that, when comparing different values of damping, they concentrated on the forces they perceived at around the center of the manipulator movement, regardless of the variation in condition settings (the center means the point where the manipulator deflection angle is zero). Because of the prescribed sinusoidal movement, this force equals the maximum damping force, as discussed in Section II, see Fig. 1. When perceiving changes in the force perceived at this point, one is actually estimating the changes in the ratio of this force to the maximum *velocity*, corresponding to the level of damping.

This strategy indicates that subjects are able to extract the damping force maximum from the combined force (for exam-

ple extracting the damping force maximum from the yellow line in Fig. 1). But the experimental observation also indicates that the perception of this force maximum is disturbed by the joint response of stiffness and mass. This is reasonable, because for a fixed level of damping b, increasing mass or stiffness yields a larger magnitude of the real projection $\Re H$, which in turn increases the magnitude of the system overall frequency response function, see Fig. 7. As a result, the effort (the force) to apply the prescribed manipulator movement also increases. This may cause more uncertainty (a higher noise level) in the force sensory channel leading to a higher force difference threshold. The increase in the damping JND is likely a consequence of this.

VII. Discussion

In this study, we extend the basic JND laws using the frequency response of JNDs for the two studied cases. In doing so, we provide a novel perspective on describing human haptic JND in their perception of mechanical properties, which may facilitate the application of such sensory characteristics to engineering design. In this section, we summarize our main findings and discuss their practical relevance, we analyze the impact of our experiment design, and discuss possible future extensions of our work.

A. Summary of results and practical relevance

1) Case 1: Stiffness JND: Our extended JND law indicates that the stiffness JND is a fixed proportion of the combined response of stiffness and mass: the "effective stiffness". In case of a mass-spring system, the effective stiffness is lower than the true stiffness level when the system is excited at a non-zero frequency, see (16). Evaluating the fidelity of a haptic interface using the traditional JND law is apparently conservative when the mass is not negligible.

2) Case 2: Damping JND: The extended JND law expresses the response of the damping JND as a fixed proportion of the system magnitude in the frequency domain. On this basis, the fidelity of the rendered damping of a haptic interface can be evaluated at individual frequencies. In most cases an increase in the manipulator damping improves the stability of the haptic interface. Our model specifies a less stringent requirement than the original law, see (17), allowing more room to balance the tradeoff between fidelity and stability.

B. Limitations of the experimental design

The results of this study were obtained from a fixed amplitude and frequency of excitation, with a side-stick manipulator. Changes in the excitation signal or the manipulator type may have different implications.

1) Excitation amplitude: In this study, the amplitude of the prescribed manipulator movement was fixed at 0.37 rad. Our proposed models still apply to other movement amplitudes that lead to moderate manipulator forces (not too high or too low), since changing this variable does not affect human capability of perceiving a force difference [10], [21]–[23]. Whereas in case of amplitudes that produce manipulator forces around the perception boundary, the ratio constant p should be adjusted.

2) Excitation frequency: The impact of the frequency needs further investigation. The model structure should not be affected by a different excitation frequency, as the principle of how humans perceive a dynamic difference from the force should be unaffected. However, the proportion of the perceivable changes – the ratio constant p in the models – may be affected by human arm's motion velocity [24] (higher frequencies are more likely to cause higher velocities). Thus, generalizing our proposed models to cases where multiple excitation frequencies are considered requires measuring the ratio constant p at each individual frequency.

3) Type of manipulator: Although the experiment was conducted with a side-stick manipulator, we believe that the proposed models also apply to other control manipulators. Again, perceiving dynamic differences from the force should be independent of the shape and size of a manipulator. However, different muscle groups may be involved when controlling a different manipulator, and this may cause a different level of force threshold [23]. Therefore measuring the ratio constant p would still be needed when applying our models to other manipulators.

C. General discussion

We find that the stiffness JND is affected by the mass, because the inertia force and spring force are coupled. This in turn, indicates that the spring stiffness affect the mass JND in the same manner. Moreover, it can be readily appreciated that the JNDs in mass and stiffness are coupled in *exactly* the same way as the coupled responses of these two mechanical properties, and that this joint JND is determined by the combined response of stiffness and mass. In addition, one can imagine that this joint JND can be also affected by the manipulator damping. We expect to use the damping JND model to describe this joint JND for cases where the system's damping property varies. This topic has indeed been considered in our ongoing research.

Although subjects interpreted the difference in both stiffness and damping from the force, the estimated ratio constants p of the two models are different (9.2% and 12.4%). This indicates that interpreting a stiffness change from the perceived force is more difficult than a damping change, as also reported in [25]. In addition, moving the undamped spring-like manipulator in the first experiment may have required our subjects to be more concentrated on the tracking task, which may also have affected the detection of a force difference. Clearly, more validation work needs to be done on this topic in the future.

VIII. Conclusion

In this study we propose models to extend the laws of JND in perceiving manipulator dynamics from force feedback. Two typical cases are considered: 1) the JND in perceiving manipulator stiffness under effects of manipulator mass; 2) the JND in perceiving manipulator damping under effects of stiffness and mass. The JND models are obtained based on a combination of frequency response functions and validated with results from psychophysical experiments. The experimental observations show that increases in mass reduce the normalized stiffness

JND (the Weber fraction for stiffness), and that increases in the combined response of stiffness and mass increases the damping JND. With the extended JND laws, all these effects can be explained. The extended JND laws indicate that the stiffness JND is a fixed proportion of the combined frequency response of stiffness and mass, i.e., the "effective stiffness", instead of the true stiffness; and that the damping JND can be expressed with Weber's law using the frequency response of the combined system as the reference stimulus.

REFERENCES

[1] D. A. Lawrence, "Stability and transparency in bilateral teleoperation," *IEEE Trans. on robotics and automation*, vol. 9, no. 5, pp. 624–637, 1993.

[2] P. H. Chang and J. Kim, "Telepresence index for bilateral teleoperations," *IEEE Trans. on Systems, Man, and Cybernetics, Part B (Cybernetics)*, vol. 42, no. 1, pp. 81–92, 2012.

[3] P. F. Hokayem and M. W. Spong, "Bilateral teleoperation: An historical survey," *Automatica*, vol. 42, no. 12, pp. 2035–2057, 2006.

[4] S. Hirche and M. Buss, "Human-oriented control for haptic teleoperation," *Proceedings of the IEEE*, vol. 100, no. 3, pp. 623–647, 2012.

[5] A. Gerretsen, M. Mulder, and M. M. Van Paassen, "Comparison of position-loop, velocity-loop and force-loop based control loading architectures," in *AIAA Modeling and Simulation Technologies Conference and Exhibit, San Francisco, CA*, 2005, pp. 1–18.

[6] W. Fu, M. M. van Paassen, and M. Mulder, "On the relationship between the force JND and the stiffness JND in haptic perception," in *Proc. of the ACM Symposium on Applied Perception*. ACM, 2017, p. 11.

[7] D. A. Abbink and M. Mulder, "Exploring the dimensions of haptic feedback support in manual control," *Journal of Computing and Information Science in Engineering*, vol. 9, no. 1, p. 011006, 2009.

[8] M. Della Penna, M. M. van Paassen, D. A. Abbink, M. Mulder, and M. Mulder, "Reducing steering wheel stiffness is beneficial in supporting evasive maneuvers," in *Proc. of the IEEE Int. Conf. on Systems Man and Cybernetics*. IEEE, 2010, pp. 1628–1635.

[9] J. Smisek, E. Sunil, M. M. van Paassen, D. A. Abbink, and M. Mulder, "Neuromuscular-system-based tuning of a haptic shared control interface for uav teleoperation," *IEEE Trans. on Human-Machine Systems*, vol. 47, no. 4, pp. 449–461, 2017.

[10] L. A. Jones, "Kinesthetic sensing," in *Human and Machine Haptics*. MIT Press, 2000.

[11] H. Z. Tan, N. I. Durlach, G. L. Beauregard, and M. A. Srinivasan, "Manual discrimination of compliance using active pinch grasp: The roles of force and work cues," *Perception & Psychophysics*, vol. 57, no. 4, pp. 495–510, 1995.

[12] L. A. Jones and I. W. Hunter, "A perceptual analysis of stiffness," *Experimental Brain Research*, vol. 79, no. 1, pp. 150–156, 1990.

[13] ——, "A perceptual analysis of viscosity," *Experimental Brain Research*, vol. 94, no. 2, pp. 343–351, 1993.

[14] G. L. Beauregard, M. A. Srinivasan, and N. I. Durlach, "The manual resolution of viscosity and mass," in *ASME Dynamic Systems and Control Division*, vol. 1, 1995, pp. 657–662.

[15] E. M. Rank, T. Schauß, A. Peer, S. Hirche, and R. L. Klatzky, "Masking effects for damping JND," in *International Conference on Human Haptic Sensing and Touch Enabled Computer Applications*. Springer, 2012, pp. 145–150.

[16] M. M. Van Paassen, J. C. Van Der Vaart, and J. A. Mulder, "Model of the neuromuscular dynamics of the human pilot's arm," *Journal of Aircraft*, vol. 41, no. 6, pp. 1482–1490, 2004.

[17] F. A. A. Kingdom and N. Prins, *Psychophysics: a Practical Introduction*. Academic Press, 2016.

[18] M. A. Garcıa-Pérez, "Forced-choice staircases with fixed step sizes: asymptotic and small-sample properties," *Vision Research*, vol. 38, no. 12, pp. 1861–1881, 1998.

[19] N. Colonnese, A. F. Siu, C. M. Abbott, and A. M. Okamura, "Rendered and characterized closed-loop accuracy of impedance-type haptic displays," *IEEE trans. on haptics*, vol. 8, no. 4, pp. 434–446, 2015.

[20] D. Findeisen, *System dynamics and mechanical vibrations: an introduction*. Springer Science & Business Media, 2013.

[21] L. A. Jones, "Matching forces: constant errors and differential thresholds," *Perception*, vol. 18, no. 5, pp. 681–687, 1989.

[22] X. D. Pang, H. Z. Tan, and N. I. Durlach, "Manual discrimination of force using active finger motion," *Perception & Psychophysics*, vol. 49, no. 6, pp. 531–540, 1991.

[23] S. Feyzabadi, S. Straube, M. Folgheraiter, E. A. Kirchner, S. K. Kim, and J. C. Albiez, "Human force discrimination during active arm motion for force feedback design," *IEEE trans. on Haptics*, vol. 6, no. 3, pp. 309–319, 2013.

[24] M. H. Zadeh, D. Wang, and E. Kubica, *Factors affecting the perception-based compression of haptic data*. INTECH Open Access Publisher, 2010.

[25] M. Rank, Z. Shi, H. J. Müller, and S. Hirche, "The influence of different haptic environments on time delay discrimination in force feedback," in *International Conference on Human Haptic Sensing and Touch Enabled Computer Applications*. Springer, 2010, pp. 205–212.

Wei Fu received the MSc degree in the faculty of Automation from Northwestern Polytechnical University, Xi'an, China, in 2015. He is currently a PhD student at the Faculty of Aerospace Engineering, TU Delft. His research interests include human-machine systems, haptic perception, haptic interface design, tele-operation and automatic control.

Annemarie Landman received her MSc in human movement sciences from the VU University, Amsterdam, the Netherlands, in 2011. She is currently a PhD student at TNO, The Netherlands, and in the faculty of Aerospace Engineering, at the Delft University of Technology.

Marinus M. (René) van Paassen received the MSc degree (*cum laude*) and PhD degree in Aerospace Engineering from TU Delft, the Netherlands, in 1988 and 1994, respectively. He is currently an associate professor at the Faculty of Aerospace Engineering, TU Delft. His research interests include human-machine systems, haptics and cognitive systems engineering. René is an associate editor of the IEEE Transactions on Human-Machine Systems.

Max Mulder received the MSc degree and PhD degree (*cum laude*) in Aerospace Engineering from TU Delft, the Netherlands, in 1992 and 1999, respectively. He is currently a full professor at the Faculty of Aerospace Engineering, TU Delft. His research interests include manual control cybernetics and ecological information systems. Max is an associate editor of the IEEE Transactions on Human-Machine Systems.